

# Observation of superspin-glass behavior in $\text{Fe}_3\text{O}_4$ nanoparticles and superparamagnetic behavior in gold-coated $\text{Fe}_3\text{O}_4$ nanoparticles

Sharbani I. Fullem<sup>†</sup>, Itsuko S. Suzuki<sup>†</sup>, Masatsugu Suzuki<sup>†§</sup>  
Lingyan Wang<sup>‡</sup>, and Chuan-Jian Zhong<sup>‡</sup>

<sup>†</sup> Department of Physics, State University of New York at Binghamton, Binghamton, New York 13902-6000, USA

<sup>‡</sup> Department of Chemistry, State University of New York at Binghamton, Binghamton, New York 13902-6000, USA

**Abstract.** The aging and memory effects of  $\text{Fe}_3\text{O}_4$  nanoparticles have been studied using a series of zero-field cooled (ZFC) and field-cooled (FC) magnetization measurements at various aging protocols. The genuine ZFC magnetization after the ZFC procedure with a single stop and wait process shows an aging dip at the stop temperature on reheating. The depth of the aging dip is dependent on the wait time. The frequency dependence of the AC magnetic susceptibility is indicative of critical slowing down at a freezing temperature  $T_f$  ( $= 30.6 \pm 1.6$  K). The relaxation time  $\tau$  is described by a power law form with a dynamic critical exponent  $x$  ( $= 8.2 \pm 1.0$ ) and a microscopic relaxation time  $\tau_0$  [ $= (1.33 \pm 0.05) \times 10^{-9}$  sec]. The ZFC-peak temperature decreases with increasing magnetic field ( $H$ ), forming a critical line with an exponent  $p = 1.78 \pm 0.26$ , close to the de Almeida-Thouless exponent ( $p = 3/2$ ). The temperature ( $T$ ) dependence of the FC and ZFC magnetic susceptibilities of gold-coated  $\text{Fe}_3\text{O}_4$  ( $\text{Fe}_3\text{O}_4@\text{Au}$ ) nanoparticles have been also measured at various  $H$ . The monotonic increase of the FC susceptibility with decreasing  $T$  is observed below the ZFC-peak temperature  $T_p$ , indicating that  $\text{Fe}_3\text{O}_4@\text{Au}$  nanoparticles exhibit a superparamagnetic behavior. The ZFC-peak temperature  $T_p$  increases with increasing  $H$ , showing a local maximum, and decreases with further increase in  $H$ . We present numerical calculations for the scaling forms of ZFC and FC susceptibilities based on the Néel-Brown model with the log-norm distribution of volumes of nanoparticles. The local maximum of the  $T_p$  vs  $H$  curve is well explained by this model with a large width of the volume distribution.

PACS numbers: 75.30.Cr, 75.40.Mg, 75.50.Lk, 75.50.Tt

<sup>§</sup> suzuki@binghamton.edu

## 1. Introduction

The aging and memory effects of ferromagnetic nanoparticles have been the focus of extensive studies in recent years [1, 2, 3, 4, 5, 6, 7, 8, 9, 10, 11, 12, 13]. Each ferromagnetic nanoparticle has a large magnetic moment (so-called superspin). Depending on the interactions between superspins, these systems are classed into two types. The noninteracting superspins give rise to superparamagnetic behavior. The superspins thermally fluctuate between their easy directions of magnetization and freeze along these directions at the blocking temperature  $T_b$ , where the relaxation time  $\tau$  becomes equal to the measuring time  $\tau_m$ . Thus the superparamagnet (SPM) has a ferromagnetic blocked state below  $T_b$ . The relaxation time typically obeys an Arrhenius law. When the interactions between superspins, which are fully frustrated and random, become sufficiently strong, the interacting superspins cause spin frustration effect, resulting in superspin glass (SSG) behavior below a freezing temperature  $T_f$ . The low temperature spin-glass (SG) phase is experimentally characterized by observation of the flatness of the FC susceptibility below  $T_f$ , a critical slowing down of the relaxation time  $\tau$  from the AC magnetic susceptibility, and a divergent behavior of the nonlinear susceptibility [3, 7]. The relaxation time  $\tau$  which can be determined from the shift of the peak temperature of the AC magnetic susceptibility  $\chi'$  (dispersion) vs temperature ( $T$ ) curve with frequency, exhibits a critical slowing down for SSG's [2, 6].

The non-equilibrium properties of SSG's and SPM's have been observed in various nanoparticle systems, as a wait time dependence of zero-field cooled (ZFC) and field cooled (FC) magnetizations under various cooling protocols [1, 2, 4, 5, 6, 8, 9, 10, 11, 12, 13]. The aging and memory effects of the SSG's are rather different from those of SPM's. A broad distribution of relaxation times characterize SPM's, while a critical slowing down occurs in the SSG's. The main features of their aging and memory effects are summarized as follows. These features provide a very unique method to determine dynamics governed by spin correlations between nanoparticles in SSG's and SPM's. (Sasaki et al. [12]).

(1) (Genuine ZFC measurement). Only for SSG's, the ZFC magnetization  $M_{ZFC}$  shows an aging dip at a stop temperature on reheating after the ZFC protocol with a single stop and wait process. The depth of the aging dip depends on the wait time  $t_w$  [8, 10, 12].  
 (2) (Genuine FC measurement). For both SSG's and SPM's, the memory effect of  $M_{FC}$  during a FC protocol with intermittent stop and wait processes are observed. A decrease of  $M_{FC}$  is observed with decreasing  $T$  for SSG's, while an increase of  $M_{FC}$  is observed with decreasing  $T$  for the SPM's [9, 11, 12, 13].

(3) (ZFC relaxation rate). Only for SSG's, the corresponding relaxation rate  $S_{ZFC}(t, t_w)$  [ $= (1/H)dM_{ZFC}/d\ln t$ ] has a peak around  $t = t_w$ , as observed in spin glasses (aging effect) [1, 5, 8].

In the present work, we have measured the ZFC susceptibility ( $\chi_{ZFC}$ ), FC susceptibility ( $\chi_{FC}$ ) and AC magnetic susceptibility ( $\chi', \chi''$ ) of  $\text{Fe}_3\text{O}_4$  nanoparticles at various cooling protocols using a SQUID (superconducting quantum interference device)

magnetometer. We show that the aging and memory effects, critical slowing down, and the flatness of the FC susceptibility at low temperatures, are clearly observed in  $\text{Fe}_3\text{O}_4$  nanoparticles. These results indicate that the SSG phase occurs below a spin freezing temperature  $T_f$  ( $= 30.6 \pm 1.6$  K). We have also measured the ZFC and FC susceptibilities of  $\text{Fe}_3\text{O}_4@\text{Au}$  nanoparticles as a function of  $T$  and  $H$ . In  $\text{Fe}_3\text{O}_4@\text{Au}$  nanoparticles, each  $\text{Fe}_3\text{O}_4$  nanoparticle as a core is wrapped by Au surface layers as a shell, leading to the increase of the interparticle spacing between core  $\text{Fe}_3\text{O}_4$  nanoparticles [14, 15]. The interparticle interaction for  $\text{Fe}_3\text{O}_4@\text{Au}$  nanoparticles is weaker than that for  $\text{Fe}_3\text{O}_4$  nanoparticles. A monotonic increase of the FC magnetic susceptibility with decreasing  $T$  below a blocking temperature  $T_b$  ( $\approx 13.5$  K) is observed in  $\text{Fe}_3\text{O}_4@\text{Au}$  nanoparticles, suggesting that the system magnetically behaves like a SPM.

The  $H$ - $T$  diagrams are examined from the temperature dependence of  $\chi_{ZFC}$  and  $\chi_{FC}$  of  $\text{Fe}_3\text{O}_4$  nanoparticles and  $\text{Fe}_3\text{O}_4@\text{Au}$  nanoparticles at various  $H$ . The peak temperatures of the ZFC susceptibility of both systems are determined as a function of  $H$ . We show that the ZFC-peak temperature  $T_p$  ( $= T_f$ ) for  $\text{Fe}_3\text{O}_4$  nanoparticles decreases with increasing  $H$ , forming a critical line with an exponent  $p = 1.78 \pm 0.26$ , close to the de Almeida-Thouless exponent ( $= 3/2$ ). This critical line is the phase boundary between the SPM and SSG phases. These results can be well described by the SSG model of interacting  $\text{Fe}_3\text{O}_4$  nanoparticle systems. In contrast,  $T_p$  of  $\text{Fe}_3\text{O}_4@\text{Au}$  nanoparticles increases with increasing  $H$ , showing a local maximum, and decreases with further increase in  $H$ . In order to understand the origin of the local maximum of  $T_p$  vs  $H$  curve, we present numerical calculations for the scaling forms of  $\chi_{ZFC}$  and  $\chi_{FC}$ , based on the Néel-Brown SPM model [16, 17] with no interaction between nanoparticles. The log-norm distribution in volumes of nanoparticles are assumed. We show that the  $T_p$  vs  $H$  curve is dependent on the width  $\sigma$  of the volume distribution: local maximum for the large  $\sigma$  and a monotonic decrease of  $T_p$  with  $H$  for the small  $\sigma$ . Our results are consistent with the calculation results reported by Kachkachi et al. [18].

The contents of the present paper are as follows. In section 2 experimental procedure is presented, including the characterization of  $\text{Fe}_3\text{O}_4$  nanoparticles and  $\text{Fe}_3\text{O}_4@\text{Au}$  nanoparticles. In section 3 we present experimental results on the ZFC susceptibility, FC susceptibility, and AC susceptibility of our systems under various cooling protocols. In section 4, we present a scaling form of the ZFC and FC susceptibilities for the SPM model by using numerical calculations. In section 5, the experimental results are discussed in light of the model calculations.

## 2. Experimental procedure

Synthesis and characterization of  $\text{Fe}_3\text{O}_4@\text{Au}$  nanoparticles and  $\text{Fe}_3\text{O}_4$  nanoparticles used in the present work has been reported in detail previously [14, 15]. These nanoparticles form domains of ordered hexagonal arrays due to high monodispersity. For synthesis of  $\text{Fe}_3\text{O}_4@\text{Au}$  nanoparticles, the  $\text{Fe}_3\text{O}_4$  nanoparticles are first synthesized as seeds. The ratio of Au precursor to iron oxide nanoparticles is approximately 7:1. The transmission

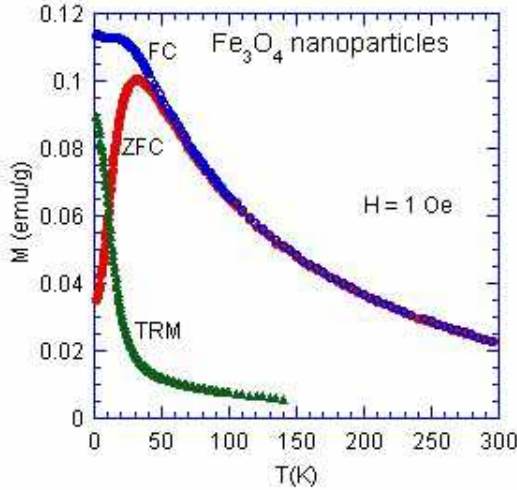


**Figure 1.** (Color online)  $T$  dependence of  $M_{ZFC}$ ,  $M_{FC}$ , and  $M_{TRM}$  for  $\text{Fe}_3\text{O}_4$  nanoparticles.  $H = 1$  Oe. The detail of the ZFC, FC, and TRM procedures is given in the text.

electron microscopy (TEM) results indicate that the size of  $\text{Fe}_3\text{O}_4$  nanoparticles is quite uniform. Their average diameter is  $52 \pm 5\text{\AA}$ .  $\text{Fe}_3\text{O}_4@\text{Au}$  nanoparticles of diameter  $63 \pm 5\text{\AA}$  consist of  $\text{Fe}_3\text{O}_4$  core of diameter  $45 \pm 5\text{\AA}$  coated with a thin layer of Au of average thickness  $9\text{\AA}$ . The approximate number of Fe atoms in each  $\text{Fe}_3\text{O}_4$  nanoparticle is roughly 2900.

The Fe ion in a  $\text{Fe}_3\text{O}_4$  nanoparticle may exist in two valencies; namely  $\text{Fe}^{2+}$  and  $\text{Fe}^{3+}$  (i.e.,  $\text{FeO}\cdot\text{Fe}_2\text{O}_3$ ). From the Curie-Weiss behavior of the DC susceptibility ( $150 \leq T \leq 298$  K and  $H = 1$  kOe) and the  $M-H$  curve at 100 K, the diameter of  $\text{Fe}_3\text{O}_4$  nanoparticles based on the assumption that they are formed of  $\text{Fe}^{3+}$  (and  $\text{Fe}^{2+}$ ) only is estimated to be  $33 \pm 5\text{\AA}$  (and  $38 \pm 5\text{\AA}$ ). This result is relatively small compared to the ones obtained from the TEM micrograph. Note that the filling factor of  $\text{Fe}_3\text{O}_4$  over the whole sample is not taken into account. The average magnetic moment of each nanoparticle is about  $3700 \mu_B$ , where  $\mu_B$  is the Bohr magneton.

The DC magnetization and AC magnetic susceptibility were measured using a SQUID magnetometer (Quantum Design, MPMS XL-5). Before the measurements, a possible remnant magnetic field was removed using ultra low field option at 298 K: the resultant remnant field was less than 3 mOe. The measurements of the DC magnetization and AC magnetic susceptibility were carried out after appropriate cooling procedures. The details of the cooling protocol for each measurement are described in section 3 and respective figure captions.

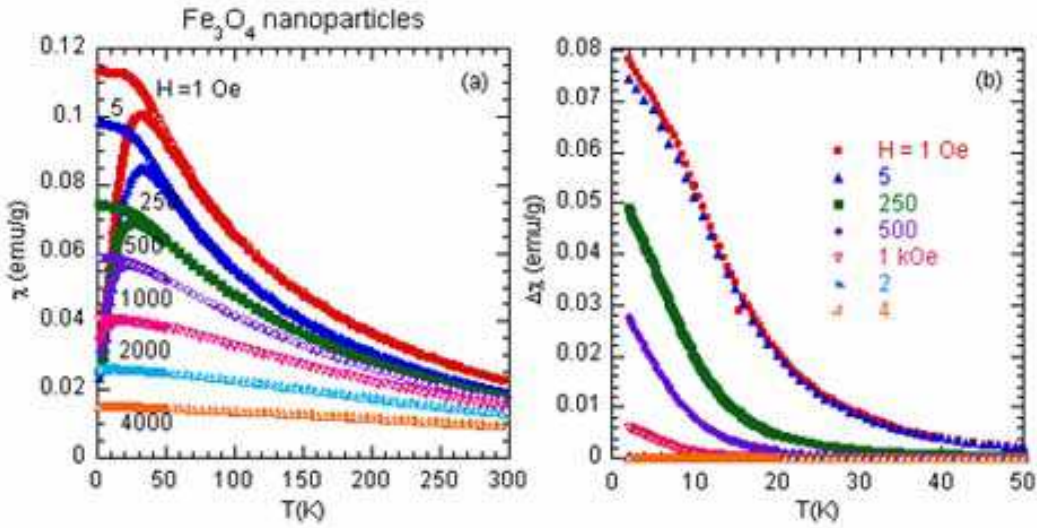


**Figure 2.** (Color online)  $T$  dependence of (a)  $\chi_{ZFC}$  and  $\chi_{FC}$ , and (b)  $\Delta\chi$  ( $= \chi_{FC} - \chi_{ZFC}$ ) of  $\text{Fe}_3\text{O}_4$  nanoparticles.  $H$  is changed as a parameter.  $1 \text{ Oe} \leq H \leq 4 \text{ kOe}$ .

### 3. Experimental result

#### 3.1. ZFC, FC and TRM magnetization of $\text{Fe}_3\text{O}_4$ nanoparticles

Figure 1 shows the  $T$  dependence of the ZFC, FC, and thermoremanent (TRM) magnetization for  $\text{Fe}_3\text{O}_4$  nanoparticles. These protocols used in the present work are explained as follows. (i) ZFC protocol: after the system was annealed at 298 K in the absence of  $H$ , it was cooled rapidly from 298 to 2.0 K. Immediately after the magnetic field  $H$  ( $= 1 \text{ Oe}$ ) was turned on at 2.0 K, the ZFC magnetization was measured with increasing  $T$  from 2.0 K to 298 K. (ii) FC protocol: After the system was annealed at 298 K in the presence of  $H$ , the FC magnetization was measured with decreasing  $T$ . (iii) TRM protocol: after the system was cooled from 298 to 2.0 K in the presence of  $H$ , the magnetic field was turned off. The TRM magnetization was then measured with increasing  $T$  from 2.0 to 100 K in the absence of  $H$ . Note that the  $T$  dependence of  $M_{ZFC}$  is similar for SSG's and SPM's, while the  $T$  dependence of  $M_{FC}$  is noticeably different for the two. The FC magnetization  $M_{FC}$  monotonically increases with increasing  $T$  for SPM's, while it tends to saturate to a constant value or even tends to decrease with decreasing  $T$  for SSG's. In this sense, the  $T$  dependence of  $M_{FC}$  is a means for distinguishing between SPM's and SSG's.

Figures 2(a) and (b) show the  $T$  dependence of  $\chi_{ZFC}$ ,  $\chi_{FC}$ , and  $\Delta\chi$  [ $= \chi_{FC} - \chi_{ZFC}$ ] for the  $\text{Fe}_3\text{O}_4$  nanoparticles at various  $H$ . The susceptibility  $\chi_{ZFC}$  at  $H = 1 \text{ Oe}$  shows a peak at  $T_p$  ( $\approx 32 \text{ K}$ ) for  $H = 1 \text{ Oe}$ . The susceptibility  $\chi_{FC}$  is almost independent of  $T$  at low temperatures well below  $T_p$ . The difference  $\Delta\chi$  gradually decreases with increasing  $T$  and starts to appear at the onset temperature of irreversibility ( $T_{irr}$ ). No sharp reduction of  $\Delta\chi$  to zero is observed at  $T = T_{irr}$ , reflecting the volume distribution

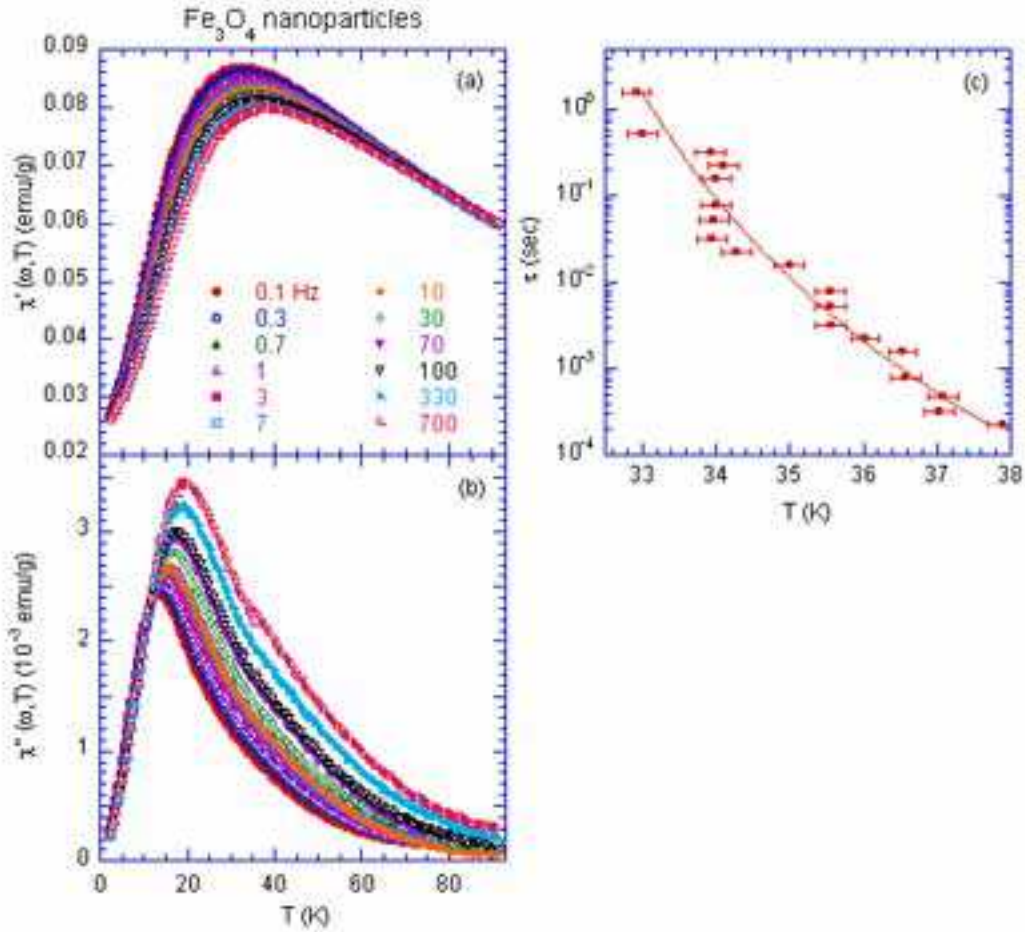


**Figure 3.** (Color online)  $T$  dependence of (a) the dispersion  $\chi'$  and (b) the absorption  $\chi''$  for  $\text{Fe}_3\text{O}_4$  nanoparticles. The frequency is changed as a parameter.  $f = 0.1 - 1000$  Hz.  $h = 0.5$  Oe.  $T = 2 - 100$  K.  $H = 0$ . (c) Relaxation time  $\tau$  ( $= 1/(2\pi f)$ ) vs  $T$  at various frequencies  $f$ .  $f = 0.1 - 1000$  Hz.  $T$  is equal to the peak temperature  $T_p(\chi')$  from  $\chi'$  vs  $T$  curve. The solid line denotes a least-squares fit of the data of  $\tau$  vs  $T$  to the power law form given by (1). The fitting parameters are given in the text.

of  $\text{Fe}_3\text{O}_4$  nanoparticles across the sample. Such a rounding effect of  $T_{irr}$  in  $\Delta\chi$  vs  $T$  disappears at a higher  $H$ . The TEM measurement shows that the size distribution of  $\text{Fe}_3\text{O}_4$  nanoparticles is similar to the log-normal distribution [14, 15]. Above  $H = 500$  Oe,  $T_{irr}$  is very close to  $T_p$ . The flatness of  $\chi_{FC}$  below  $T_p$  and the coinciding of  $T_{irr}$  and  $T_p$  suggest that the  $\text{Fe}_3\text{O}_4$  nanoparticles exhibit a SSG-like behavior.

### 3.2. AC magnetic susceptibility of $\text{Fe}_3\text{O}_4$ nanoparticles

Figures 3(a) and (b) show the  $T$  dependence of the AC magnetic susceptibility: (a) the dispersion  $\chi'$  and (b) the absorption  $\chi''$  at  $H = 0$ . After the system was annealed at 298 K in the absence of  $H$ , it was rapidly cooled from 298 to 2.0 K. Both  $\chi'$  and  $\chi''$  were measured at a fixed  $T$  ( $T \geq 2.0$  K) for various frequencies between 0.1 and

1000 Hz. After each measurement, the temperature was increased by  $\Delta T$ . The same measurement was then repeated at the temperature  $T + \Delta T$ . As shown in figure 3(a),  $\chi'$  at  $f = 0.1$  Hz shows a relatively broad peak at a peak temperature  $T_p(\chi')$  ( $= 32.5$  K). This peak shifts to the high- $T$  side with increasing  $f$ :  $T_p(\chi') = 38.5$  K for  $f = 1$  kHz. Also, the peak height of  $\chi'$  increases with increasing  $f$ . As shown in figure 3(b), in contrast, the absorption  $\chi''$  at  $f = 0.1$  Hz shows a relatively sharp peak at a peak temperature  $T_p(\chi'')$  ( $= 13.5$  K). This peak shifts to the high- $T$  side with increasing  $f$ :  $T_p(\chi'') = 20$  K for  $f = 1$  kHz. The peak height of  $\chi''$  decreases with increasing  $f$ . It should be noted that  $\chi''$  is independent of  $f$  below 12 K.

It is empirically known that the frequency shift in the peak temperature  $T_p(\chi')$  of  $\chi'$  vs  $T$  curve, defined by  $\Gamma = (1/T_p)\Delta T_p/\Delta(\log_{10} \omega)$ , offers a good criterion for distinguishing SG's ( $\Gamma < 0.06$ ) from SPM's ( $\Gamma \approx 0.3$ ) [19]. Our value of  $\Gamma$  can be estimated as  $\Gamma \approx 0.05$ , which suggests that our system is a SSG, and not a SPM. According to Hansen et al [6], there are two criteria for the determination of the freezing temperature. First, the freezing temperature is defined as the temperature at which  $\chi''$  attains 15% of its maximum value. Second, the freezing temperature is defined from the relation  $\chi'(\omega, T_f) = 0.98\chi_{FC}(T = T_f)$ . Nevertheless, for convenience here we define the freezing temperature as the peak temperature  $T_p(\chi')$ . Figure 3(c) shows the relaxation time  $\tau$  which is estimated as  $\tau = 1/(2\pi f)$  as a function of  $T$  [ $= T_p(\chi')$ ]. The least-squares fit of the data of  $\tau$  vs  $T$  to a power law form for the critical slowing down,

$$\tau = \tau_0(T/T_f - 1)^{-x}, \quad (1)$$

yields a dynamic critical exponent  $x = 8.2 \pm 1.0$ , a microscopic relaxation time  $\tau_0 = (1.33 \pm 0.5) \times 10^{-9}$  sec, and a freezing temperature  $T_f = 30.6 \pm 1.6$  K. Our values of  $x$  and  $\tau_0$  are comparable with those of the Fe-C nanoparticles with a volume concentration 15 vol % (superspin glass) reported by Hansen et al. [6]:  $x = 9.5$  and  $\tau_0 = 5.0 \times 10^{-9}$  sec. Note that our value of  $x$  is also in good agreement with that of the 3D Ising spin glass  $\text{Fe}_{0.5}\text{Mn}_{0.5}\text{TiO}_3$  ( $x = 9.3 \pm 1.0$ ) [20]. These results indicate that our system is a SSG.

### 3.3. Memory effect in FC magnetization in $\text{Fe}_3\text{O}_4$ nanoparticles

We present a peculiar memory effect observed in  $\text{Fe}_3\text{O}_4$  nanoparticles using a unique FC aging protocol. This effect also provides a good measure for determining whether the system is a SPM or a SSG [12]. Figure 4 shows the memory effect of the FC magnetization which is measured in the following way. First, the system was cooled using the FC protocol from 298 K to intermittent stop temperatures  $T_s$  ( $= 23, 20, 17, 14, 11, 8$ , and 5 K) in the presence of  $H$  ( $= 5$  Oe). When the system was cooled down to each  $T_s$ , the field was turned off ( $H = 0$ ) and the system was aged at  $T_s$  for a wait time  $t_s$  ( $= 1.0 \times 10^4$  sec). The FC magnetization denoted by  $M_{FC}^{IS}(T \downarrow)$  decreases with time  $t$  due to the relaxation, where  $IS$  stands for intermittent stop. After each wait time  $t_s$  at  $T_s$ , the field ( $H = 5$  Oe) was turned on and the cooling was resumed. We find that such an aging process leads to a step-like behavior of  $M_{FC}^{IS}(T \downarrow)$

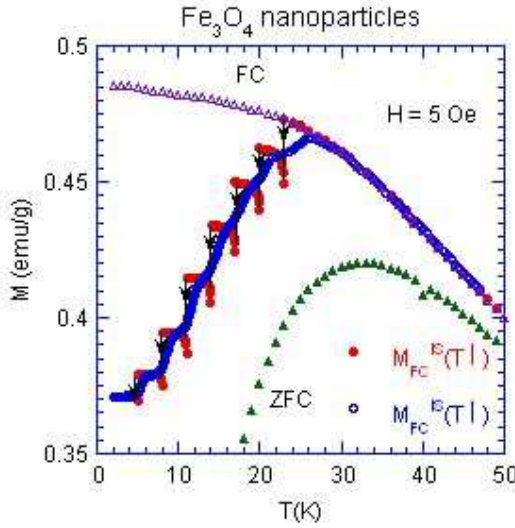


**Figure 4.** (Color online)  $T$  dependence of  $M_{FC}^{IS}(T \downarrow)$  (●) and  $M_{FC}^{IS}(T \uparrow)$  (○) for  $\text{Fe}_3\text{O}_4$  nanoparticles, observed in the following FC aging protocol. The system is quenched from 298 to 50 K in the presence of  $H$  (= 5 Oe).  $M_{FC}^{IS}(T \downarrow)$  is measured with decreasing  $T$  from 50 to 2.0 K but with intermittent stops (IS) at  $T_s = 23, 20, 17, 14, 11, 8$ , and 5 K for a wait time  $t_s = 1.0 \times 10^4$  sec. The field is cut off during each stop. The arrows indicate the relaxation of  $M_{FC}^{IS}(T \downarrow)$ .  $M_{FC}^{IS}(T \uparrow)$  is measured at  $H = 5$  Oe with increasing  $T$  after the above cooling process. The  $T$  dependence of  $M_{FC}^{ref}$  (Δ) and  $M_{ZFC}^{ref}$  (▼) are also shown as reference curves.

curve. Immediately after reaching 2.0 K, the magnetization  $M_{FC}^{IS}(T \uparrow)$  was measured in the presence of  $H$  (= 5 Oe) as the temperature was increased at a constant rate of 0.05 K/min. The magnetization  $M_{FC}^{IS}(T \uparrow)$  thus measured exhibits step-like changes at each  $T_s$ . This implies that the spin configuration imprinted at each intermittent stop at  $T_s$  for the wait time  $t_s$  at  $H = 0$  is retrieved by the curve on reheating. The magnetization  $M_{FC}^{IS}(T \downarrow)$  is either parallel to  $M_{FC}^{ref}$  as a reference at temperatures near  $T_s = 23$  and 20 K or is independent of  $T$  at temperatures near  $T_s = 14, 11, 8$ , and 5 K. The magnetization  $M_{FC}^{ref}(T \downarrow)$  without intermittent stops is almost constant or even tends to decrease with decreasing  $T$ . The magnetization  $M_{FC}^{IS}(T \downarrow)$  with intermittent stops decreases with decreasing  $T$ , while  $M_{FC}^{IS}(T \uparrow)$  increases with increasing  $T$ . They meet together at temperatures a little above each stop temperature (approximately 1 K). Similar memory effects in the FC magnetization have been observed in the SSG  $\text{Fe}_3\text{N}$  nanoparticles [12]. These features are in contrast to that of the SPM's such as ferritin (Sasaki et al. [12], and Mamiya et al. [4]), permalloy  $\text{Ni}_{81}\text{Fe}_{19}$  (Sun et al. [9]), Co particles (Zheng et al. [11]): both  $M_{FC}^{IS}(T \downarrow)$  with intermittent stops and  $M_{FC}^{ref}(T \downarrow)$  without intermittent stops monotonically increase with decreasing  $T$ .

In summary, the decrease of  $M_{FC}^{IS}(T \downarrow)$  with decreasing  $T$  is a feature common to SSG's, while the increase of  $M_{FC}^{IS}(T \downarrow)$  with decreasing  $T$  is a feature common to SPM's.

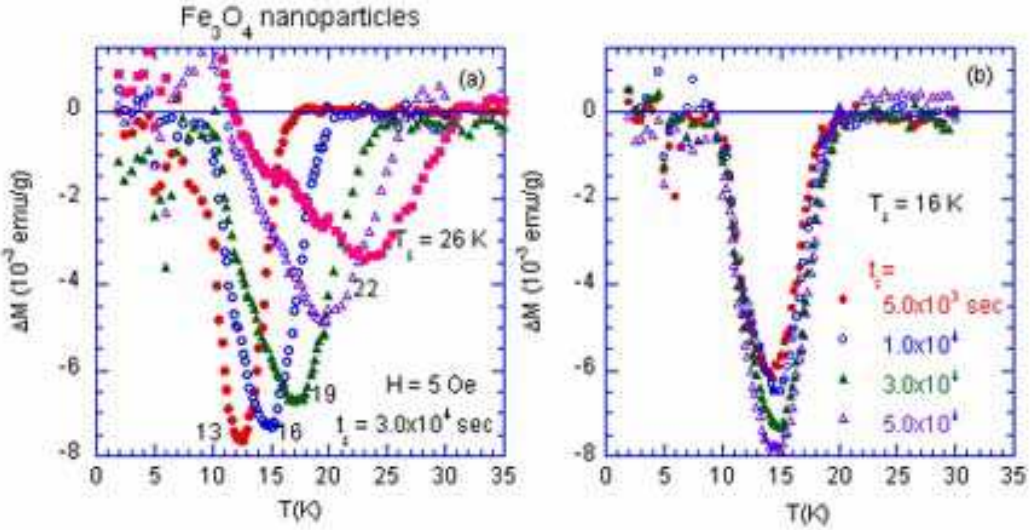


**Figure 5.** (Color online) (a)  $T$  dependence of the genuine ZFC susceptibility for  $\text{Fe}_3\text{O}_4$  nanoparticles.  $\Delta\chi_{ZFC} = \chi_{ZFC}^{SSW}(T \uparrow) - \chi_{ZFC}^{ref}(T \uparrow)$ . The system was annealed at  $T = 100$  K for 1200 sec. After the system was quickly cooled from 100 K to  $T_s$  at  $H = 0$ , it was aged at a stop temperature  $T_s$  ( $= 26, 22, 19, 16$ , and  $13$  K) for a wait time  $t_s = 3.0 \times 10^4$  sec [single stop and wait (SSW) process]. The cooling was resumed from  $T_s$  to  $2.0$  K. Immediately after the field was turned on, the ZFC susceptibility  $\chi_{ZFC}^{SSW}(T \uparrow)$  was measured at  $H = 5$  Oe with increasing  $T$ . The reference ZFC susceptibility  $\chi_{ZFC}^{ref}(T \uparrow)$  was measured at  $H = 5$  Oe after the ZFC protocol without any stop and wait process. (b)  $T$  dependence of  $\Delta\chi_{ZFC}$ .  $T_s = 16$  K.  $t_s = 5.0 \times 10^4, 3.0 \times 10^4, 1.0 \times 10^4, 5.0 \times 10^3$  and  $2.0 \times 10^3$  sec. The ZFC protocol was the same as used in (a).

### 3.4. Memory effect in ZFC magnetization in $\text{Fe}_3\text{O}_4$ nanoparticles

We measured the ZFC susceptibility of  $\text{Fe}_3\text{O}_4$  nanoparticles after the ZFC aging protocol with a single-stop and wait (SSW) procedure. The sample was first rapidly cooled in zero-magnetic field from 100 K down to a stop temperature  $T_s$ . The system was aged at  $T_s$  for a wait time  $t_s$ . The cooling was then resumed down to 2.0 K. Immediately after the magnetic field was turned on, the ZFC susceptibility  $\chi_{ZFC}^{SSW}(T \uparrow)$  was measured on reheating. The reference ZFC magnetization  $\chi_{ZFC}^{ref}(T \uparrow)$  was also measured after the direct cooling of the system from 100 to 2.0 K without any stop and wait process. Figure 5(a) shows the  $T$  dependence of the difference defined by  $\Delta\chi_{ZFC}^{SSW}(T \uparrow) = \chi_{ZFC}^{SSW}(T \uparrow) - \chi_{ZFC}^{ref}(T \uparrow)$  for the SSW process, where  $T_s = 16.0$  K and  $H = 5$  Oe. The wait times are chosen as  $t_s = 5.0 \times 10^3, 1.0 \times 10^4, 3.0 \times 10^4$ , and  $5.0 \times 10^4$  sec, respectively. We find that the difference  $\Delta\chi_{ZFC}^{SSW}(T \uparrow)$  takes a local minimum (an aging dip) at 15.9 K just below  $T_s$ . When the system is isothermally aged at  $T_s = 16.0$  K for  $t_s$ , its spin configuration gets arranged towards the equilibrium state. With further decrease in  $T$ , the equilibrated state becomes frozen in and the memory is retrieved on reheating. The depth of the aging dip is dependent on  $t_s$ , showing a clear evidence of the aging behavior that the domain size grows with time. We find here that the depth

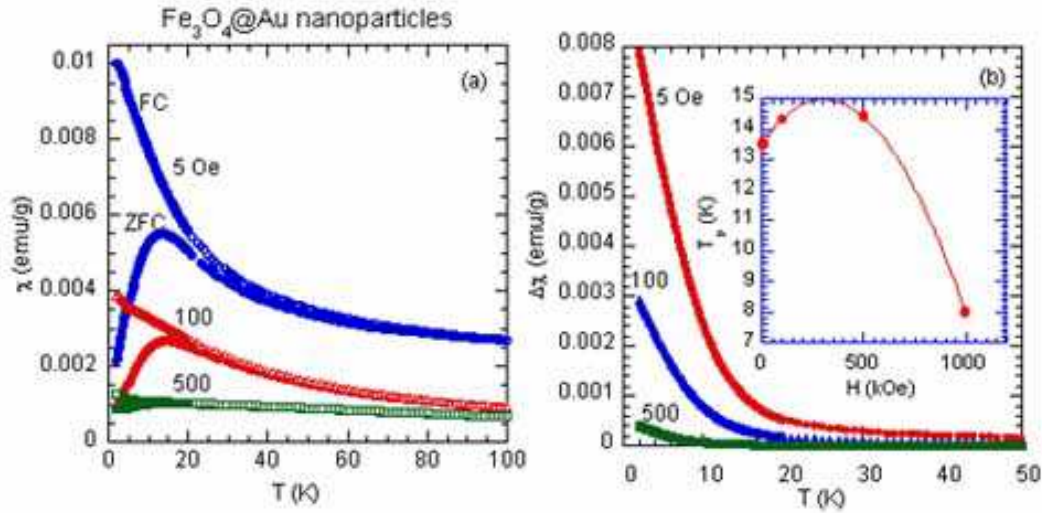


**Figure 6.** (Color online)  $T$  dependence of (a)  $\chi_{ZFC}$  and  $\chi_{FC}$ , and (b)  $\Delta\chi$  of  $\text{Fe}_3\text{O}_4@\text{Au}$  nanoparticles.  $H$  is changed as a parameter.  $H = 5, 100$ , and  $500$  Oe. The inset of (b) shows the plot of  $T_p$  as a function of  $H$  for  $\text{Fe}_3\text{O}_4@\text{Au}$  nanoparticles.  $T_p$  is the ZFC-peak temperature. The solid line is a guide to the eyes.

changes with increasing  $t_s$  according to a power law form given by

$$|\Delta\chi_{ZFC}^{SSW}|_{dip} = At_s^b, \quad (2)$$

with  $A = 0.0026 \pm 0.0002$  and  $b = 0.10 \pm 0.01$ . Similar aging dip has been observed in the ZFC susceptibility in a metal-insulator multilayer [ $\text{Co}_{80}\text{Fe}_{20}(0.9\text{nm})/\text{Al}_2\text{O}_3(3\text{nm})]_{10}$  [8, 10] (SSG) and a 3D Ising SG  $\text{Fe}_{0.5}\text{Mn}_{0.5}\text{TiO}_3$  [21]. In  $\text{Fe}_{0.5}\text{Mn}_{0.5}\text{TiO}_3$ , the depth of the aging dip logarithmically changes with  $t_s$ , rather than a power law form. We notice that our value of  $b$  is nearly equal to the exponent  $b''$  obtained from the time dependence of the absorption  $\chi''(\omega, t)$  ( $= A''t^{-b''}$ ) for  $\text{Fe}_{0.5}\text{Mn}_{0.5}\text{TiO}_3$ :  $b'' = 0.14 \pm 0.03$  [22].

Figure 5(b) shows the  $T$  dependence of the difference  $\Delta\chi_{ZFC}$  at  $H = 5$  Oe for the SSW process at  $T_s$  ( $= 13, 16, 19, 22$ , and  $26$  K) for a wait time  $t_s$  ( $= 3.0 \times 10^4$  sec) during the ZFC protocol. The difference  $\Delta\chi_{ZFC}$  clearly shows an aging dip. This dip occurs at the stop temperature  $T_s$  where the system is aged during the SSW process. This result indicates the occurrence of the aging behavior. The depth of the aging dip is the largest at  $T_s = 13.0$  K and decreases with further increase in  $T_s$ . The width of the aging dip becomes broader as the stop temperature  $T_s$  increases for  $13 \leq T_s \leq 26$  K. Since the aging dip is expected to disappear for  $T_s$  above  $T_f$ , this result indicates that the freezing temperature  $T_f$  is at least higher than  $T_s = 26$  K. In fact, this result is consistent with our estimation of  $T_f$  ( $= 30.6 \pm 1.6$  K) which is derived in section 3.2.

### 3.5. ZFC and FC susceptibility of $\text{Fe}_3\text{O}_4@\text{Au}$ nanoparticles

Figures 6(a) and (b) show the  $T$  dependence of  $\chi_{ZFC}$ ,  $\chi_{FC}$ , and  $\Delta\chi [= \chi_{FC} - \chi_{ZFC}]$  for  $\text{Fe}_3\text{O}_4@\text{Au}$  nanoparticles, for  $H = 5, 100$  and  $500$  Oe, respectively. The onset

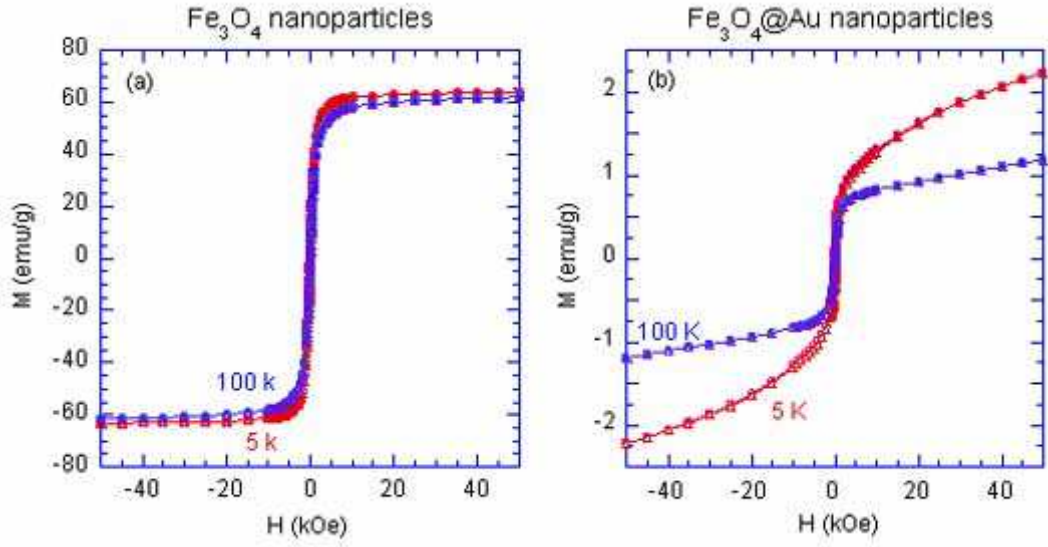


**Figure 7.** (Color online)  $M$ - $H$  curves for (a)  $\text{Fe}_3\text{O}_4$  nanoparticles and (b)  $\text{Fe}_3\text{O}_4@\text{Au}$  nanoparticles at  $T = 5$  and  $100$  K. The measurement is made after the ZFC protocol (cooling the system from  $298$  K to  $T$  in the absence of  $H$ ). The magnetization  $M$  is measured as a function of  $H$ , where  $H$  is changed as follows: (i)  $H = 0 \rightarrow 50$  kOe, (ii)  $H = 50 \rightarrow -50$  kOe, and (iii)  $H = -50 \rightarrow 50$  kOe.

temperature of irreversibility  $T_{irr}$  occurs far away from the peak temperature of  $\chi_{ZFC}$  ( $T_p$ ); close to the annealing temperature of the sample. The peak temperature  $T_p$  is regarded as the blocking temperature  $T_b$  for the superparamagnet. The susceptibility  $\chi_{FC}$  does not become constant below  $T_p$  but continues to increase with decreasing  $T$ . The peak height of  $\chi_{ZFC}$  in  $\text{Fe}_3\text{O}_4@\text{Au}$  nanoparticles is much lower than that for  $\text{Fe}_3\text{O}_4$  nanoparticles. In the inset of figure 6(b), we show the plot of  $T_p$  as a function of  $H$  for  $\text{Fe}_3\text{O}_4@\text{Au}$  nanoparticles. The ZFC-peak temperature  $T_p$  increases slightly with increasing  $H$  at low  $H$ , showing a peak around  $H = 350$  Oe, and it decreases with further increasing  $H$ .

### 3.6. $M$ vs $H$ for $\text{Fe}_3\text{O}_4$ nanoparticles and $\text{Fe}_3\text{O}_4@\text{Au}$ nanoparticles

Figures 7(a) and 8(a), and figures 7(b) and 8(b) show the magnetization hysteresis curves ( $M$  vs  $H$ ) of  $\text{Fe}_3\text{O}_4$  nanoparticles and  $\text{Fe}_3\text{O}_4@\text{Au}$  nanoparticles at  $T = 5$  and  $100$  K, respectively. The measurements were made after the ZFC protocol [the cooling of the system from  $298$  K to  $T$  ( $= 5$  or  $100$  K)] in the absence of  $H$ . The hysteresis curve at  $5$  K for  $\text{Fe}_3\text{O}_4@\text{Au}$  nanoparticles shows a pinched shape around  $H = 0$ . It is rather different from the hysteresis curve at  $5$  K for  $\text{Fe}_3\text{O}_4$  nanoparticles. No magnetic hysteresis is observed at  $100$  K for both systems. The magnetization curve of  $\text{Fe}_3\text{O}_4$  nanoparticles at  $T = 100$  K is well described by

$$M = M_s^0 L(x), \quad (3)$$

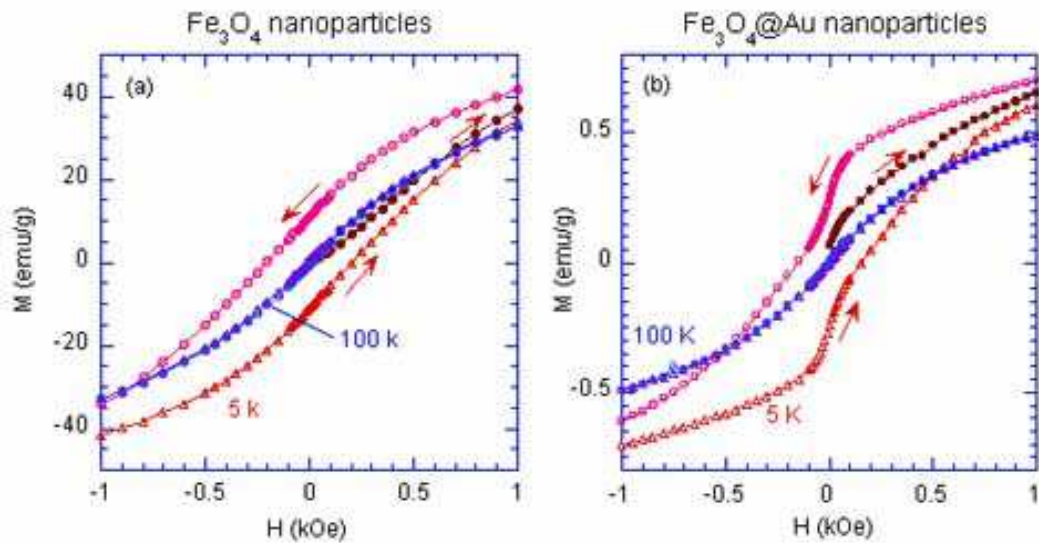


**Figure 8.** (Color online) Detaile of  $M$ - $H$  curves (figures 7(a) and (b)) for  $-1 \leq H \leq 1$  kOe. (a)  $\text{Fe}_3\text{O}_4$  nanoparticles and (b)  $\text{Fe}_3\text{O}_4@\text{Au}$  nanoparticles.

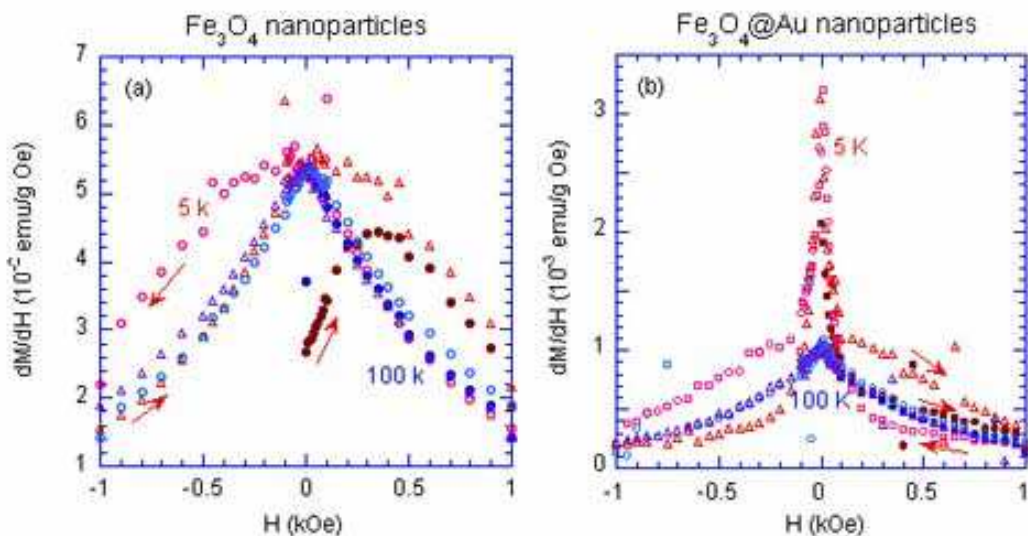


**Figure 9.** (Color online)  $dM/dH$  vs  $H$  for (a)  $\text{Fe}_3\text{O}_4$  nanoparticles and (b)  $\text{Fe}_3\text{O}_4@\text{Au}$  nanoparticles at  $T = 5$  and  $100\text{ K}$ . The curves of  $dM/dH$  vs  $H$  are obtained from the derivative of the magnetic hysteresis loops of figures 8(a) and (b) with respect to  $H$ .

with  $x = Ng\mu_BS/k_BT$ , where  $L(x)$  is the Langevin function

$$L(x) = \coth(x) - \frac{1}{x}, \quad (4)$$

$g = 2$ ,  $S = 5/2$  (for  $\text{Fe}^{3+}$ ),  $M_s^0$  is the saturation magnetization per gram ( $\approx 61$  emu/g), and  $N$  is estimated as 750. This implies that  $\text{Fe}_3\text{O}_4$  nanoparticles exhibit a SPM behavior at  $T = 100$  K. In contrast, the magnetization curve of  $M$  vs  $H$  for  $\text{Fe}_3\text{O}_4@\text{Au}$  nanoparticles at  $T = 100$  K does not have a good fit for the Langevin function at the high- $H$  side, partly because of possible additional linear contribution to the magnetization. Figures 9(a) and (b) show the plot of  $dM/dH$  as a function of  $H$  at  $T = 5$  and 100 K for  $\text{Fe}_3\text{O}_4$  nanoparticles and  $\text{Fe}_3\text{O}_4@\text{Au}$  nanoparticles, respectively, where the  $dM/dH$  vs  $H$  curves are obtained from the derivative of the  $M$ - $H$  hysteresis loops with respect to  $H$ . Note that the  $H$  dependence of  $dM/dH$  vs  $H$  at  $T = 5$  K for  $\text{Fe}_3\text{O}_4@\text{Au}$  nanoparticles is rather different from that at  $T = 100$  K. It shows a very sharp peak near  $H = 0$ . In contrast, the  $H$  dependence of  $dM/dH$  at  $T = 5$  K for  $\text{Fe}_3\text{O}_4$  nanoparticles is similar to that at  $T = 100$  K. It shows a broad peak at  $H = 0$ . We will show that the sharp peak of  $dM/dH$  (ZFC) vs  $H$  at  $H = 0$  as well as the increase of  $T_p$  with increasing  $H$  at small  $H$  in  $\text{Fe}_3\text{O}_4@\text{Au}$  nanoparticles is well explained in terms of our theory presented below.

#### 4. Scaling form of ZFC and FC susceptibility in a superparamagnet

##### 4.1. Néel-Brown model

We present a numerical calculation of the  $T$  dependence of the ZFC and FC susceptibility for SPM's where no dipole-dipole interaction is taken into account between adjacent nanoparticles. The  $T$  dependence of  $\chi_{ZFC}$  and  $\chi_{FC}$  for  $\text{Fe}_3\text{O}_4@\text{Au}$  nanoparticle (SPM) will be discussed based on these numerical calculations.

Let us consider a single-domain magnetic nanoparticle with uniaxial anisotropy. The variable part of the energy is given by  $F = \Delta E_a(V) \sin^2 \theta$ , where  $\theta$  is the angle between the direction of magnetization and the easy axis. The direction of minimum energy corresponds to  $\theta = 0$  or  $\pi$ . These directions are separated by an energy barrier of height  $\Delta E_a(V) = K_u V$  where  $K_u$  is the uniaxial anisotropy constant and  $V$  is the volume of nanoparticle. In the Néel-Brown relaxation process [16, 17], the relaxation time of the magnetization between the two states is given by,

$$\tau = \tau_0 \exp\left[\frac{\Delta E_a(V)}{k_B T}\right], \quad (5)$$

where  $\tau_0$  is a microscopic limiting relaxation time (usually  $\tau_0 \approx 10^{-9}$  sec). The measurement time  $\tau_m$  is typically of the order of  $10^2$  sec for the DC magnetization measurement. In (5) with  $\tau = \tau_m$  and  $T = T_b(V)$ , the blocking temperature  $T_b(V)$  is derived as

$$T_b(V) = \frac{\Delta E_a(V)}{k_B \ln(\tau_m/\tau_0)}. \quad (6)$$

In the presence of an external magnetic field  $H$ , it is assumed that the energy barrier  $\Delta E_a(V, H)$  is described by

$$\Delta E_a(V, H) = K_u V (1 - h)^\alpha, \quad (7)$$

where  $h = H/H_K$ ,  $H_K$  is the anisotropy field defined by  $H_K = 2K_u/M_s$ , and  $M_s$  is the saturation magnetization of the particle per unit volume. Here we assume  $\alpha = 2$ . Note that  $\alpha = 1.5$  when the orientational order is taken into account [23]. The blocking temperature  $T_b(V, H)$  is given by

$$T_b(V, H) = \frac{K_u V}{k_B \ln(\tau_m/\tau_0)} (1 - h)^\alpha. \quad (8)$$

Here we assume that all nanoparticles have the same volume  $V$ . Above the blocking temperature  $T_b(V, H)$ , the system is in the SPM state. The magnetization  $M^{spm}$  (per unit volume) for the SPM state is given by [24],

$$M_{ZFC}^{spm}(V) = M_{FC}^{spm}(V) = \epsilon M_s L \left( \frac{M_s V H}{k_B T} \right), \quad (9)$$

where  $\epsilon$  is the volume fraction occupied by ferromagnetic nanoparticles.

Below  $T_b(V, H)$ , the system is in a blocked state. The magnetization  $M^{bl}$  (per unit volume) of the ferromagnetic blocked state is given by [24]

$$M_{ZFC}^{bl}(V) = \frac{\epsilon M_s^2 H}{3 K_u}, \quad (10)$$

and

$$M_{FC}^{bl}(V) = \epsilon M_s L \left( \frac{M_s V H}{k_B T_b(V, H)} \right). \quad (11)$$

We consider a system of ferromagnetic nanoparticles having a wide distribution of volume sizes and let  $\langle V \rangle$  be their average volume. We also define a characteristic volume  $V_m(T, H)$  given by

$$V_m(T, H) = \frac{k_B T}{K_u (1 - h)^\alpha} \ln(\tau_m/\tau_0), \quad (12)$$

which is derived from the condition

$$\frac{\Delta E_a(H, V_m)}{k_B T} = \ln(\tau_m/\tau_0). \quad (13)$$

For simplicity we introduce a volume ratio  $x$  ( $= V/\langle V \rangle$ ). The characteristic volume ratio  $x_m$  is then defined by

$$x_m = \frac{V_m(T, H)}{\langle V \rangle} = \frac{k_B T}{K_u \langle V \rangle (1 - h)^\alpha} \ln(\tau_m/\tau_0) = \frac{y}{(1 - h)^\alpha} \ln(\tau_m/\tau_0), \quad (14)$$

where  $y$  is the reduced temperature and is defined by  $y = k_B T/(K_u \langle V \rangle)$ . For  $x < x_m$ , the system is in a SPM state, and for  $x > x_m$ , the system is in a blocked state. For the SPM state, the ZFC and FC magnetizations shown in (9) can be rewritten as

$$M_{ZFC}^{spm}(x, y, h) = M_{FC}^{spm}(x, y, h) = \epsilon M_s L \left( \frac{2hx}{y} \right), \quad (15)$$

while for the blocked state (10) and (11) are rewritten as

$$M_{ZFC}^{bl}(x, y, h) = \epsilon M_s \frac{2h}{3}, \quad (16)$$

and

$$M_{FC}^{bl}(x, y, h) = \epsilon M_s L \left( \frac{2h}{(1-h)^\alpha} \ln(\tau_m/\tau_0) \right), \quad (17)$$

respectively.

We assume that volume distribution of the nanoparticles,  $f(x, \sigma)$ , is expressed by the log-normal function [24],

$$f(x, \sigma) = \frac{1}{\sqrt{2\pi}\sigma x} \exp\left[-\frac{(\ln x)^2}{2\sigma^2}\right], \quad (18)$$

where  $\sigma$  is the width of the log-normal volume distribution function. Using (15)–(18), the scaling forms of the ZFC and FC susceptibility are given by

$$\frac{\chi_{ZFC}(y, h, \sigma)}{\chi_0} = \frac{1}{h} \int_0^\infty \left[ L\left(\frac{2hx}{y}\right) U_{-1}(x_m - x) + \frac{2h}{3} U_{-1}(x - x_m) \right] f(x, \sigma) dx, \quad (19)$$

and

$$\frac{\chi_{FC}(y, h, \sigma)}{\chi_0} = \frac{1}{h} \int_0^\infty \left[ L\left(\frac{2hx}{y}\right) U_{-1}(x_m - x) + L\left(2h \frac{\ln(\tau_m/\tau_0)}{(1-h)^\alpha}\right) U_{-1}(x - x_m) \right] f(x, \sigma) dx, \quad (20)$$

where  $U_{-1}$  is a step function [ $U_{-1}(x) = 1$  for  $x \geq 0$  and  $0$  for  $x < 0$ ].  $\chi_0$  [ $= \epsilon M_s^2 / (2K_u)$ ] is a constant susceptibility and  $x_m$  given by (14) is a function of  $y$ ,  $h$ , and  $\tau_m/\tau_0$ . The normalized ZFC and FC susceptibilities depend only on  $y$ ,  $h$ ,  $\tau_m/\tau_0$ , and  $\sigma$ . They are independent of the values of  $\epsilon$ ,  $M_s$ ,  $K_u$ , and  $\langle V \rangle$ .

#### 4.2. Numerical calculation

Figures 10(a)–(f) show typical plots of  $\chi_{ZFC}/\chi_0$ ,  $\chi_{FC}/\chi_0$  and the difference  $\delta$  defined by  $\delta = (\chi_{ZFC} - \chi_{FC})/\chi_0$  as a function of the normalized temperature ( $y = k_B T / K_u \langle V \rangle$ ), where  $\alpha = 2.0$  and  $\ln(\tau_m/\tau_0) = 25.328$ . The reduced field  $h$  ( $= H/H_K$ ) is kept constant at  $h = 0.1$ , and the width of the log-normal volume distribution function ( $\sigma$ ) is varied as a parameter ( $\sigma = 0.1$  to  $0.6$ ). The normalized ZFC susceptibility  $\chi_{ZFC}/\chi_0$  for  $\sigma = 0.1$  exhibits a peak at the normalized ZFC-peak temperature  $y_p$ . The difference  $\delta$  starts to appear at the onset temperature of irreversibility  $y_{irr}$  (just above  $y_p$ ) and increases with decreasing  $y$ . The irreversible effect of susceptibility occurs below  $y_{irr}$ . The normalized FC susceptibility  $\chi_{FC}/\chi_0$  for  $\sigma = 0.1$  is nearly independent of  $y$  below  $y_p$ . These features are common to those observed in real SG systems [24]. Here, the system behaves like a SSG, where the large magnetic moment of the nanoparticle plays the same role as an atomic spin in a SG system. As  $\sigma$  increases, the peak of  $\chi_{ZFC}/\chi_0$  becomes broad and shifts to the large  $y$ -side. The normalized FC susceptibility  $\chi_{FC}/\chi_0$  for large  $\sigma$  (typically  $\sigma = 0.6$ ) tends to increase with decreasing  $y$  in the small- $y$  region (at low temperatures).

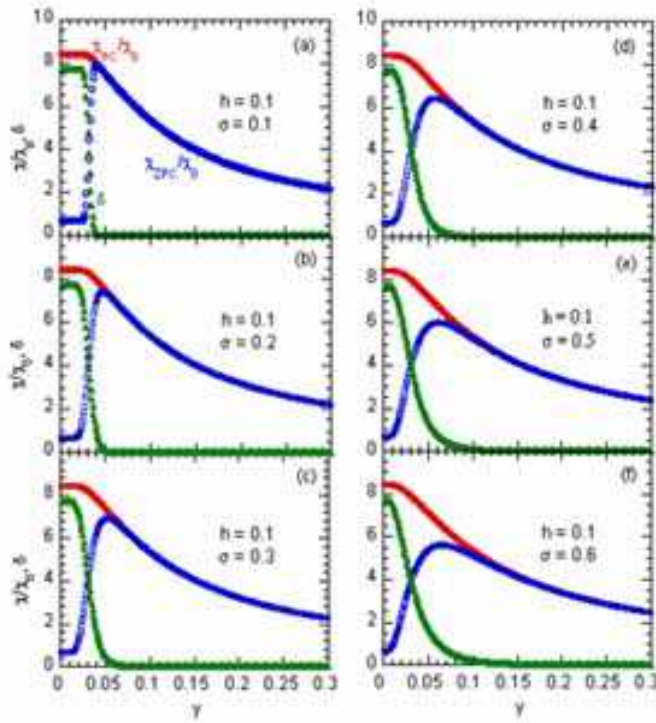


**Figure 10.** (Color online) Plot of  $\chi_{ZFC}/\chi_0$ ,  $\chi_{FC}/\chi_0$ , and  $\delta = (\chi_{FC} - \chi_{ZFC})/\chi_0$  as a function of reduced temperature  $y$ .  $h = 0.1$ . The width  $\sigma$  is varied from 0.1 to 0.6 as a parameter.  $\alpha = 2.0$ .

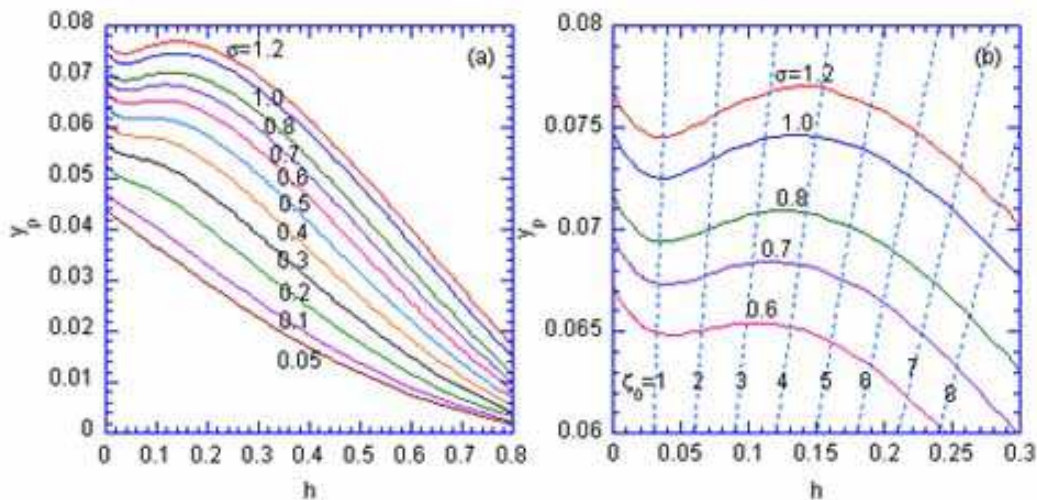


**Figure 11.** (Color online) (a)  $y_p$  vs  $h$  diagram at various  $\sigma$  ( $= 0.05 - 1.2$ ).  $y_p$  is the normalized ZFC-peak temperature, and  $h$  is the normalized field.  $\alpha = 2.0$ .  $\sigma$  is the width of the log-norm distribution. (b) Detail of the  $y_p$  vs  $h$  diagram at  $\sigma = 0.6, 0.7, 0.8, 1.0$ , and  $1.2$ . The dotted lines are denoted by  $y_p = 2h/\zeta_0$  with  $\zeta_0 = 1, 2, \dots, 8$ .

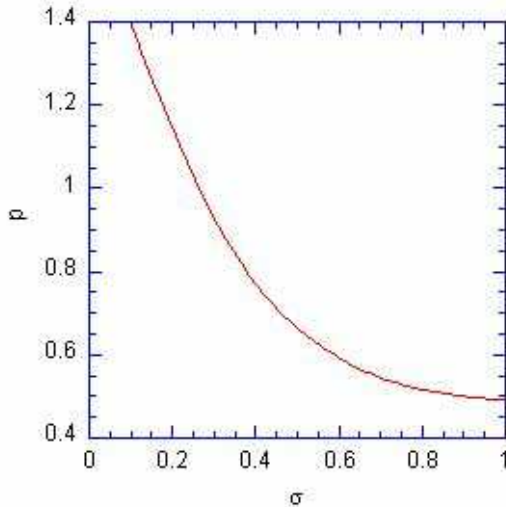


**Figure 12.** (Color online) Exponent  $p$  vs  $\sigma$ . The exponent  $p$  is derived from the least-squares fit of the  $y_b$  vs  $h$  curves for  $0.1 \leq h \leq 0.6$  to (21).  $\alpha = 2.0$ .

Figures 11(a) and (b) show a plot of  $y_p$  as a function of  $h$  at various width  $\sigma$ . For a small width (typically  $\sigma \leq 0.11$ ),  $y_p$  monotonically decreases with increasing  $h$ . At a larger width (typically  $0.6 \leq \sigma \leq 1.2$ ) for very low  $h$ ,  $y_p$  decreases with increase in  $h$ , and shows a local minimum around  $h = 0.05$ . On the other hand, for higher  $h$  (at larger  $\sigma$ ) it increases with increasing  $h$ , showing a local maximum around  $h = 0.10 - 0.15$ , and decreases with further increasing  $h$ . The local maximum position shifts to high- $h$  side with increasing  $\sigma$ . The origin of the local maximum in the  $y_p$  vs  $h$  curves may arise mainly due to the nonlinearity of the Langevin function in (19), as will be discussed in section 5. It should be noted that this  $y_p$  vs  $h$  diagram may be a feature common to any SPM's, since it depends only on the scaled variables  $h$  and  $y$ .

As shown in figure 11(a), the curvature of  $y_p$  vs  $h$  curve drastically changes with varying  $\sigma$ . We assume that the  $h$  dependence of  $y_p$  is expressed by a power law form

$$h = h_0 \left(1 - \frac{y_p}{y_0}\right)^p, \quad (21)$$

for  $0.1 \leq h \leq 0.6$ , where  $p$  is an exponent and  $h_0$  and  $y_0$  are constants. The least-squares fit of the numerical result of  $h$  vs  $y_p$  for each  $\sigma$  to (21) yields the parameters  $p$ ,  $y_0$ , and  $h_0$ . In figure 12, we show the value of  $p$  thus obtained, as a function of  $\sigma$ . We find that the exponent  $p$  is strongly dependent on the width  $\sigma$ :  $p$  increases with decrease in  $\sigma$ . The exponent  $p$  is nearly equal to 0.5 at  $\sigma = 1.2$ . It increases with decreasing  $\sigma$  and is nearly equal to 1.5 at  $\sigma = 0.01$ . Note that  $p = 3/2$  is an exponent predicted for the de Almeida-Thouless (AT) line [25] for the  $H$ - $T$  diagram in Ising SG systems.

Figure 13(a) shows the plot of  $y_p(\sigma, h)$  as a function of  $\sigma$  for a fixed  $h$  ( $= 0.001 - 0.4$ ). The value of  $y_p$  increases with increasing  $\sigma$  at each  $h$ . Figure 13(b) shows the ratio  $\mu$  defined as  $\mu = y_p(\sigma, h)/y_p(\sigma = 0, h)$  as a function of  $\sigma$  at various  $h$ , where  $y_p(\sigma = 0, h)$  is obtained from the extrapolation of  $y_p(\sigma, h)$  in the limit of  $\sigma \rightarrow 0$ . We find that the

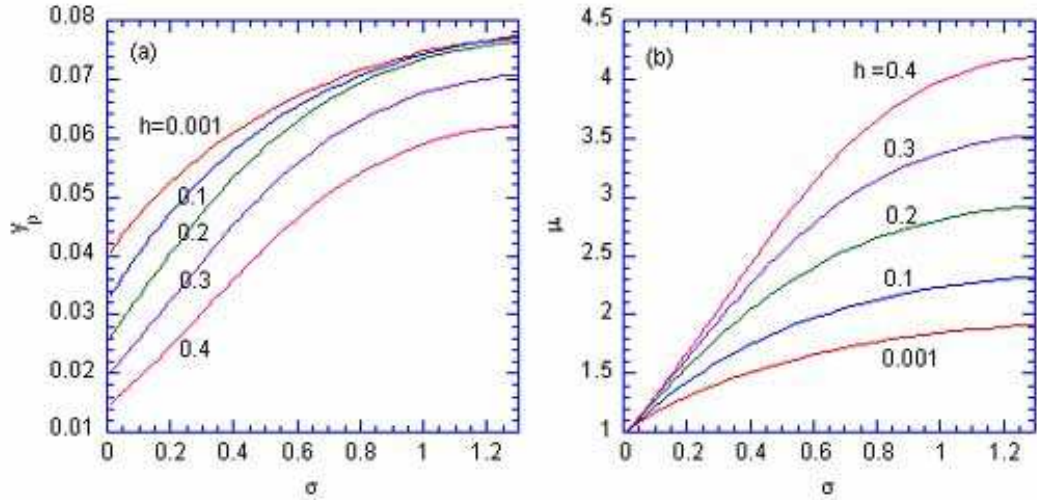


**Figure 13.** (Color online) (a)  $y_p(\sigma, h)$  vs  $\sigma$  at  $h = 0.001, 0.1, 0.2, 0.3$ , and  $0.4$ .  $\alpha = 2.0$ . (b) Plot of  $\mu = y_p(\sigma, h)/y_p(\sigma \rightarrow 0, h)$  vs  $\sigma$  at various  $h$ .

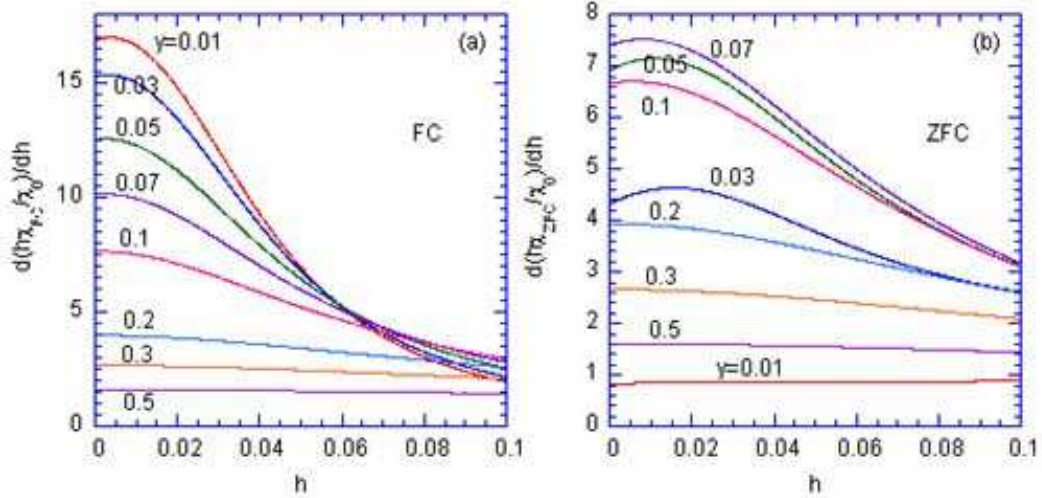


**Figure 14.** (Color online)  $h$ -dependence of  $d(h\chi_{FC}/\chi_0)/dh$  and  $d(h\chi_{ZFC}/\chi_0)/dh$  at various  $y$  ( $= 0.01 - 0.4$ ).  $\sigma = 0.6$ .  $\alpha = 2.0$ .

ratio  $\mu$  is proportional to  $\sigma$  at small  $\sigma$  and tends to saturate at large  $\sigma$ . Our result is very different from the prediction by Sappey et al. [23] above  $\sigma = 0.8$ . Their value of  $\mu$  tends to diverge with increasing  $\sigma$  above  $\sigma = 0.8$ , while that of ours tends to saturate. The reason for such a difference in  $\mu$  at large  $\sigma$  is that the nonlinearity of the Langevin function with  $y$  and  $h$  is not taken into account in the paper by Sappey et al. [23].

Figure 14(a) shows the  $h$  dependence of the derivative  $d(h\chi_{FC}/\chi_0)/dh$  at various  $y$ . It shows a peak at  $h = 0$  for any  $y$ , where  $\sigma = 0.6$ . The peak height at  $h = h_p = 0$  drastically decreases with increasing  $y$ . Figure 14(b) shows the  $h$  dependence of the

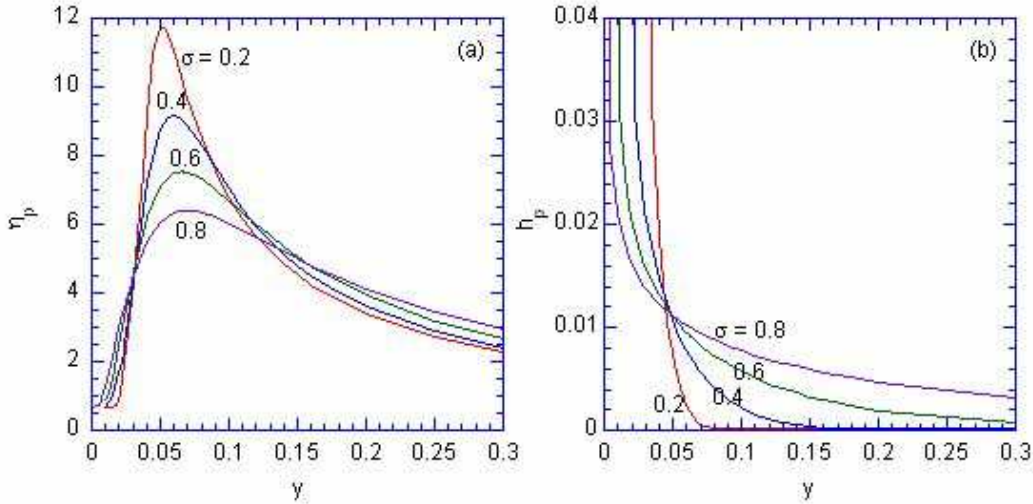


**Figure 15.** (Color online) (a) The peak height  $\eta_p$  and (b) the peak field  $h_p$  as a function of  $y$  at various  $\sigma$ , where  $d(h\chi_{ZFC}/\chi_0)/dh$  vs  $h$  curve exhibits a peak height  $\eta_p$  at a peak field  $h_p$  for each  $y$ .  $\alpha = 2.0$ .

derivative  $d(h\chi_{ZFC}/\chi_0)/dh$  at various  $y$ . It shows a broad peak at  $h = h_p$  ( $= 0.0159$ ) for  $y = 0.03$ , where  $\sigma = 0.6$ . This peak field  $h_p$  shifts to the lower- $h$  side with increasing  $y$ , while the peak height  $\eta_p$  increases with increasing  $y$ , showing a local maximum at  $h_p = 0.0089$  ( $\simeq 0$ ) for  $y \approx 0.065$ . We note that these values of  $y$  and  $h_p$  for the local maximum are located on the  $y_p$  vs  $h$  diagram ( $h \simeq 0$ ) for  $\sigma = 0.6$  (see figure 11(b)). Figures 15(a) and (b) show the peak height  $\eta_p$  and the peak field  $h_p$  as a function of  $y$  at various  $\sigma$  for  $d(h\chi_{ZFC}/\chi_0)/dh$  vs  $h$ , respectively. The peak height  $\eta_p$  shows a local maximum around  $h = 0.05 - 0.06$ . The peak field  $h_p$  decreases with increasing  $y$ . These features are independent of  $\sigma$ .

In summary, we obtain the following important features from the above numerical calculations. (i) The ZFC susceptibility  $\chi_{ZFC}/\chi_0$  vs  $y$  has a broad peak at  $y = y_p$ , forming the  $y_p$  vs  $h$  diagram. The value of  $y_p$  exhibits a local minimum and a local maximum for a large  $\sigma$ . (ii) The derivative  $d(h\chi_{ZFC}/\chi_0)/dh$  vs  $h$  shows a very sharp peak around  $h = 0$  at low  $y$ . (iii) The derivative  $d(h\chi_{ZFC}/\chi_0)/dh$  vs  $h$  shows a peak at the boundary of the  $(y_p, h)$  phase diagram ( $h \simeq 0$ ). (iv) Monotonic increase of  $\chi_{ZFC}/\chi_0$  with decreasing  $y$  is seen below  $y_p$  for relatively large  $\sigma$ . With decreasing  $\sigma$ ,  $\chi_{ZFC}/\chi_0$  becomes flat below  $y_p$ .

## 5. Discussion

### 5.1. ZFC-peak temperature and $\partial M_{FC}/\partial H$ in SPM $Fe_3O_4@Au$ nanoparticles

Both the non-monotonic  $H$  dependence for the ZFC-peak temperature  $T_p$  [23, 26, 27, 28, 29, 30, 31] and the sharp peak of the derivative  $dM/dH$  have been observed in many SPM's [27, 29, 32]. Several theories have been presented for the explanation of

the maximum of  $T_p$  at low  $H$  [18, 23, 33, 34] including the theories based on the Néel-Brown model [18, 23, 31, 34] and the resonant spin tunneling theory [33]. The peak of  $T_p$  at small  $H$  in  $\text{Mn}_{12}\text{O}_{12}(\text{CH}_3\text{COO})_{16}(\text{H}_2\text{O})_4$  (denoted as  $\text{Mn}_{12}$ ) [28] and ferritin [27] is explained in terms of thermally assisted, field-tuned resonant tunneling between particles. However, this model may not be valid for the explanation of similar behaviors in SPM's with  $T_p$  which is too high for the quantum effect to appear.

In section 4 we show that these features can be well explained in terms of the scaling form of  $\chi_{ZFC}/\chi_0$  and  $\chi_{FC}/\chi_0$ . The local minimum and local maximum of  $y_p$  tends to disappear as  $\sigma$  becomes smaller. The non-monotonic behavior of  $y_b$  is mainly due to the non-linearity of the Langevin function. The curvature of  $y_b$  vs  $h$  is strongly dependent on  $\sigma$ . It is interesting to discuss where the nonlinearity of the Langevin function is significant in the  $y_p$  vs  $h$  plane. Note that  $\chi_{ZFC}/\chi_0$  is given by (19) using the Langevin function which is a function of

$$\zeta = (M_s V) H / (k_B T) = 2hx/y, \quad (22)$$

where  $x = V/\langle V \rangle$ ,  $y = k_B T/(K_u \langle V \rangle)$ ,  $h = H/H_k$ , and  $H_k = 2K_u/M_s$ .  $M_s V$  is the magnetic moment of the particle of volume  $V$  and  $M_s$  is its magnetization per unit volume. The nonlinearity is considered to appear when  $\zeta > 1$ . For convenience we assume that  $x = 1$ , which means  $V = \langle V \rangle$ . Then  $\zeta$  is approximated as  $\zeta = \zeta_0 = 2h/y$ . In figure 11(a), we make a plot of the straight lines denoted by the relation  $\zeta_0 = 2h/y$  ( $= 1-8$ ). It is clear that the local maximum and local minimum for each  $\sigma$  are located on the lines with  $\zeta_0 = 1$  and  $\zeta_0 = 3-4$ . This implies that the nonlinearity of the Langevin function is crucial to the occurrence of the local maximum and local minimum. In the numerical calculation, Sappey et al. [23] have used the approximation of the Langevin function for  $\zeta \ll 1$ , which may lead to results inconsistent with our numerical results. We note that  $y_p$  with  $\sigma > 0.4$  exhibits a local minimum around  $h = 0$  as shown in figure 11(a). This local minimum is located around the line given by  $\zeta_0 = 1$  in the  $y_p$  vs  $h$  curve with each  $\sigma$ . Experimentally Luis et. al [30] have reported that in natural horse-spleen ferritin the curve of  $T_p$  vs  $H$  exhibits a local minimum at  $H = 0.5$  kOe and a maximum at  $H = 3$  kOe. This result is qualitatively consistent with the results of our numerical calculation.

It is interesting to estimate the value of  $\zeta$  at which the  $T_p$  vs  $H$  curve for the  $\text{Fe}_3\text{O}_4@\text{Au}$  nanoparticle exhibits a maximum ( $T_p = 13.0$  K and  $H_p = 300$  Oe). We note that each  $\text{Fe}_3\text{O}_4$  nanoparticle has about  $\mu = 3700\mu_B$ . All spins are ferromagnetically ordered in each nanoparticle. This value of  $\zeta$  is estimated as  $\zeta = 0.25(H_p/T_p) = 5.7$ . Here the appearance of the peak is closely related to the nonlinearity of the Langevin function.

In the present work, we find that the  $dM/dH$  (ZFC) vs  $H$  curve at  $T = 5.0$  K in  $\text{Fe}_3\text{O}_4@\text{Au}$  nanoparticles shows a very sharp peak around  $H = 0$ . Tejada et al [27] have also reported the  $M-H$  (ZFC) curve in ferritin at  $T = 5$  and 13 K. The derivative  $dM/dH$  vs  $H$  exhibits a very sharp peak at  $H = 0$  for  $T = 5$  and 13 K. The peak height at  $T = 13$  K close to  $T_p$  ( $\approx 13.7$  K) at  $H \approx 0$ , is much larger than that at  $T =$

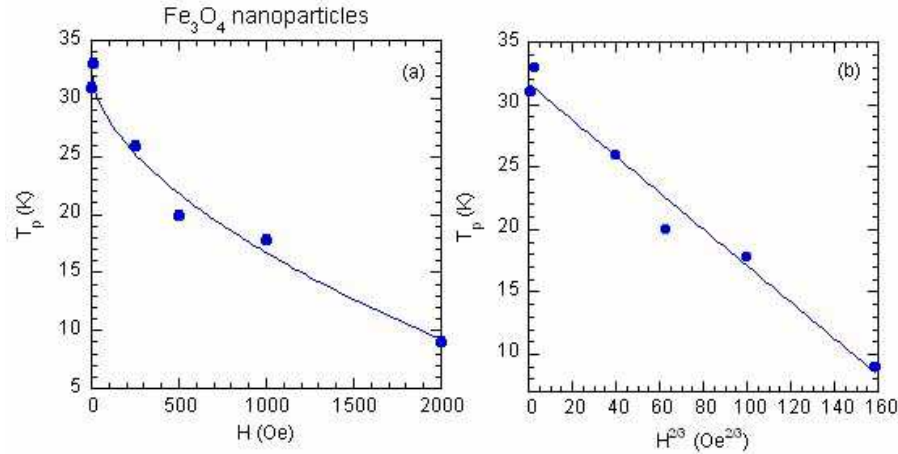


**Figure 16.** (Color online) (a) Plot of  $T_p$  as a function of  $H$  for  $\text{Fe}_3\text{O}_4$  nanoparticles.  $T_p$  is a temperature at which  $\chi_{ZFC}$  exhibits a peak. The solid line is least-squares fitting curve to (23) with  $T_g = 32.5 \pm 1.4$  K,  $H_0 = 3.61 \pm 0.71$  kOe, and  $p = 1.78 \pm 0.36$ . (b) Plot of  $T_p$  as a function of  $H^{2/3}$  for  $\text{Fe}_3\text{O}_4$  nanoparticles. The straight line denotes a least-squares fitting curve to (24) with  $T_f = 31.69 \pm 0.97$  K and  $H_0 = 3.20 \pm 0.30$  kOe.

5 K. These results are in good agreement with our prediction from figure 14(b) for the  $d(h\chi_{ZFC}/\chi_0)/dh$  vs  $h$  curves at various  $y$  and  $\sigma$ .

### 5.2. AT transition in SSG $\text{Fe}_3\text{O}_4$ nanoparticles

In the mean-field picture, the phase transition of the SG systems can survive in the presence of low  $H$ , forming a critical line, the so-called de Almeida-Thouless (AT) line in the  $H$ - $T$  phase diagram [25]

$$H(T) = H_0(1 - T/T_f)^p, \quad (23)$$

where  $T_f$  is the spin freezing temperature,  $H_0$  is a field amplitude and the exponent  $p = 3/2$ . This line is the phase boundary between the PM (paramagnetic) phase and the SG phase. The correlation length and relaxation times diverge on crossing this line. In figure 16(a) we show the plot of the ZFC-peak temperature  $T_p$  of  $\chi_{ZFC}$  vs  $T$  as a function of  $H$  for  $\text{Fe}_3\text{O}_4$  nanoparticles. The peak temperature  $T_p$  decreases with increasing  $H$ . This critical line in the  $H$ - $T_p$  diagram may correspond to the phase boundary between the SPM and SSG phases. The least-squares fit of the data of  $H$  vs  $T_p$  for  $1 \text{ Oe} \leq H \leq 2 \text{ kOe}$  to (23) yields the parameters  $p = 1.78 \pm 0.26$ ,  $T_f = 32.5 \pm 1.4$  K, and  $H_0 = 3.61 \pm 0.71$  kOe. We find that  $p$  is close to the AT exponent ( $p = 3/2$ ). Figure 16(b) shows a plot of  $T_p$  as a function of  $H^{2/3}$ . It seems that all the data of  $T_p$  vs  $H^{2/3}$  fall well on a straight line given by

$$T_p = T_f[1 - H^{2/3}/H_0^{2/3}], \quad (24)$$

where  $T_f = 31.69 \pm 0.97$  K and  $H_0 = 3.20 \pm 0.30$  kOe. These results indicate that there is an AT critical line in the  $H$ - $T$  phase diagram for  $\text{Fe}_3\text{O}_4$  nanoparticles as a SSG

system. Note that  $T_p$  is equal to  $T_{irr}$  in an ideal SSG system. The field  $H_0$  of the AT line for the SSG system is given by [35]

$$H_0 = \frac{2}{\sqrt{3}} \frac{k_B T_f}{N g \mu_B S}, \quad (25)$$

where  $N g \mu_B S$  is used instead of  $g \mu_B S$  in the original equation. Like an Ising SG system, the value of  $N$  is estimated as  $N = 34$ , where  $H_0 = 3.2$  kOe,  $T_f = 31.69$  K,  $g = 2$ , and  $S = 5/2$ . The value of  $N$  thus obtained is much smaller than that evaluated from the different methods (see section 2). Here we note that similar AT critical line has been reported by Sahoo et al. [7] for ferromagnetic single domain particles of CoFe in discontinuous magnetic layers (Co<sub>80</sub>Fe<sub>20</sub>/Al<sub>2</sub>O<sub>3</sub> multilayers). This system undergoes a SSG transition at a spin freezing temperature  $T_f$ . The peak temperature  $T_p$  of the ZFC susceptibility shifts to the low- $T$  side with increasing  $H$ . The least-squares fit of the data of  $T_p$  vs  $H$  in the low-field range to (23) yields the exponent  $p$  ( $= 1.5 \pm 0.4$ ), which is close to the AT exponent ( $p = 3/2$ ). In conclusion, the nature of the AT line in SSG systems is essentially the same as that in the SG systems.

The above discussion is based on the mean-field picture. The situation is rather different in the droplet picture [36]. It is predicted that no phase transition occurs in the presence of even an infinitesimal  $H$  as in the case of a ferromagnet. So there is no AT line in the  $H$ - $T$  phase diagram. Any apparent transition would be an artifact related to the limited experimental time scale. Several experimental results support the prediction from the droplet picture; the instability of the SG phase in thermal equilibrium in a finite  $H$  [37, 38].

## 6. Conclusion

The aging and memory effects of Fe<sub>3</sub>O<sub>4</sub> nanoparticles have been studied in a series of DC magnetization measurements using various cooling protocols. The genuine FC magnetization after the FC procedure with multiple intermittent stop and wait processes shows a step-like increase at each stop temperature on reheating. The genuine ZFC magnetization after the ZFC procedure with a single intermittent stop and wait process shows an aging dip at the stop temperature on reheating. The depth of the aging dip is dependent on the wait time. The frequency dependence of the AC magnetic susceptibility for Fe<sub>3</sub>O<sub>4</sub> nanoparticles is indicative of critical slowing down at a freezing temperature  $T_f$  ( $= 30.6 \pm 1.6$  K). The flatness of the FC susceptibility is observed below the ZFC-peak temperature  $T_p$ . The  $H$  dependence of  $T_p$  for Fe<sub>3</sub>O<sub>4</sub> nanoparticles forms a critical line with an exponent  $p = 1.78 \pm 0.26$ , close to the de Almeida-Thouless exponent ( $= 3/2$ ). These results are well described by the SSG model of interacting Fe<sub>3</sub>O<sub>4</sub> nanoparticle system.

The FC and ZFC magnetic susceptibilities of Au coated Fe<sub>3</sub>O<sub>4</sub> nanoparticles have been measured. We find that Fe<sub>3</sub>O<sub>4</sub>@Au nanoparticles exhibit a superparamagnetic behavior. The susceptibility is characterized by an increase in  $\chi_{FC}$  below the ZFC-peak temperature  $T_p$  with decreasing temperature. The  $H$ - $T$  diagrams for Fe<sub>3</sub>O<sub>4</sub>@Au

nanoparticles are compared with numerical calculations on the scaling form of ZFC and FC susceptibility based on the SPM blocking model. We find that the overall features of the FC and ZFC susceptibility of  $\text{Fe}_3\text{O}_4@\text{Au}$  nanoparticles can be well explained in terms of the SPM blocking model.

## Acknowledgments

The preparation of nanomaterials was supported by National Science Foundation (CHE 0349040).

## References

- [1] Jonsson T, Mattsson J, Djurberg C, Khan F A, Nordblad P and Svedlindh P 1995 *Phys. Rev. Lett.* **75** 4138
- [2] Djurberg C, Svedlindh P, Nordblad P, Hansen M F, Bødker F, and Mørup S 1997 *Phys. Rev. Lett.* **79** 5154
- [3] Jonsson T, Svedlindh P and Hansen M F 1998 *Phys. Rev. Lett.* **81** 3976
- [4] Mamiya H, Nakatani I and Furubayashi T 1998 *Phys. Rev. Lett.* **80** 177
- [5] Jönsson P, Hansen M F, and Nordblad P 2000 *Phys. Rev. B* **61** 1261
- [6] Hansen M F, Jönsson P E, Nordblad P and Svedlindh P 2002 *J. Phys.: Condens. Matter* **14** 4901
- [7] Sahoo S, Petracic O, Binek Ch, Kleemann W, Sousa J B, Cardoso S and Freitas P P 2002 *Phys. Rev. B* **65** 134406
- [8] Sahoo S, Petracic O, Kleemann W, Nordblad P, Cardoso S and Freitas P P 2003 *Phys. Rev. B* **67** 214422
- [9] Sun Y, Salamon M B, Garnier K and Averback R S 2003 *Phys. Rev. Lett.* **91** 167206
- [10] Sahoo S, Petracic O, Kleemann W, Nordblad P, Cardoso S and Freitas P P 2004 *J. Magn. Magn. Mater.* **272-276** 1316
- [11] Zheng R K, Hongwei Gu and Zhang X X 2004 *Phys. Rev. Lett.* **93** 139702
- [12] Sasaki M, Jönsson P E, Takayama H and Mamiya H 2005 *Phys. Rev. B* **71** 104405
- [13] Tsoi G M, Wenger L E, Senaratne U, Tackett R J, Buc E C, Naik R, Vaishnava P P and Naik V 2005 *Phys. Rev. B* **72** 014445
- [14] Wang L, Luo J, Maye M, Fan Q, Rendeng Q, Engelhard M, Wang C, Lin Y and Zhong C J 2005 *J. Mater. Chem.* **15** 1821
- [15] Wang L, Luo J, Fan Q, Suzuki M, Suzuki I S, Engelhard M H, Lin Y, Kim N, Wang J Q and Zhong C J 2005 *J. Phys. Chem. B* **109** 21593
- [16] Néel L, 1949 *Compt Rend. (Paris)* **228** 604
- [17] Brown W F Jr 1963 *Phys. Rev.* **130** 1677
- [18] Kachkachi H, Coffey W T, Crothers D S F, Ezzir A, Kennedy E C, Nogues M and Tronc E 2000 *J. Phys.: Condens. Matter* **12** 3077
- [19] Mydosh J A 1993 *Spin glasses: an experimental introduction* (London: Taylor & Francis)
- [20] Gunnarsson K, Svedlindh P, Nordblad P, Lundgren L, Aruga H and Ito A 1988 *Phys. Rev. Lett.* **61** 754
- [21] Mathieu R, Jönsson P E, Nordblad P, Katori H A and Ito A 2001 *Phys. Rev. B* **65** 012411
- [22] Dupuis V, Vincent E, Bouchaud J-P, Hammann J, Ito A and Katori H A 2001 *Phys. Rev. B* **64** 174204
- [23] Sappey R, Vincent E, Hadacek N, Chaput F, Boilot J P and Zins D 1997 *Phys. Rev. B* **56** 14551
- [24] Bitoh T, Ohba K, Takamatsu M, Shirane T and Chikazawa S 1995 *J. Phys. Jpn.* **64** 1305
- [25] de Almeida J R L and Thouless D J 1978 *J. Phys. A* **11** 983
- [26] Luo W, Nagel S R, Rosenbaum T F and Rosensweig R E 1991 *Phys. Rev. Lett.* **67** 2721

- [27] Tejada J, Zhang X X, del Barco D, Hernández J M and Chudnovsky E M 1997 *Phys. Rev. Lett.* **79** 1754
- [28] Friedman J R, Sarachik M P, Tejada J and Ziolo R 1996 *Phys. Rev. Lett.* **76** 3830
- [29] Friedman J R, Voskoboynik U and Sarachik M P 1997 *Phys. Rev. B* **56** 10793
- [30] Luis F, del Barco E, Hernández J M, Remiro E, Bartolomé J, and Tejada J 1999 *Phys. Rev. B* **59** 11837
- [31] Zheng R K, Gu H, Xu B, Zhang X X 2006 *J. Phys.: Condens. Matter* **18** 5905
- [32] Zhang X X, Hemandez J M, Tejada J and Ziolo R F 1996 *Phys. Rev. B* **54** 4101
- [33] Chudnovsky E M 1998 *J. Mag. Mag. Mater.* **185** L267
- [34] Chantrell R W, Walmsley N, Gore J and Maylin M 2000 *Phys. Rev. B* **63** 024410
- [35] Katori H A and Ito A 1994 *J. Phys. Soc. Jpn.* **63** 3122
- [36] Fisher D S and Huse D A 1986 *Phys. Rev. Lett.* **56** 1601; 1988 *Phys. Rev. B* **38** 373; 1988 *Phys. Rev. B* **38** 386
- [37] Mattsson J, Jonsson T, Nordblad P, Katori H A and Ito A 1995 *Phys. Rev. Lett.* **74** 4305
- [38] Suzuki I S and Suzuki M 2005 *Phys. Rev. B* **72** 104429